iScience

CellPress
OPEN ACCESS

Article

The deubiquitinase cofactor UAF1 interacts with USP1 and plays an essential role in spermiogenesis

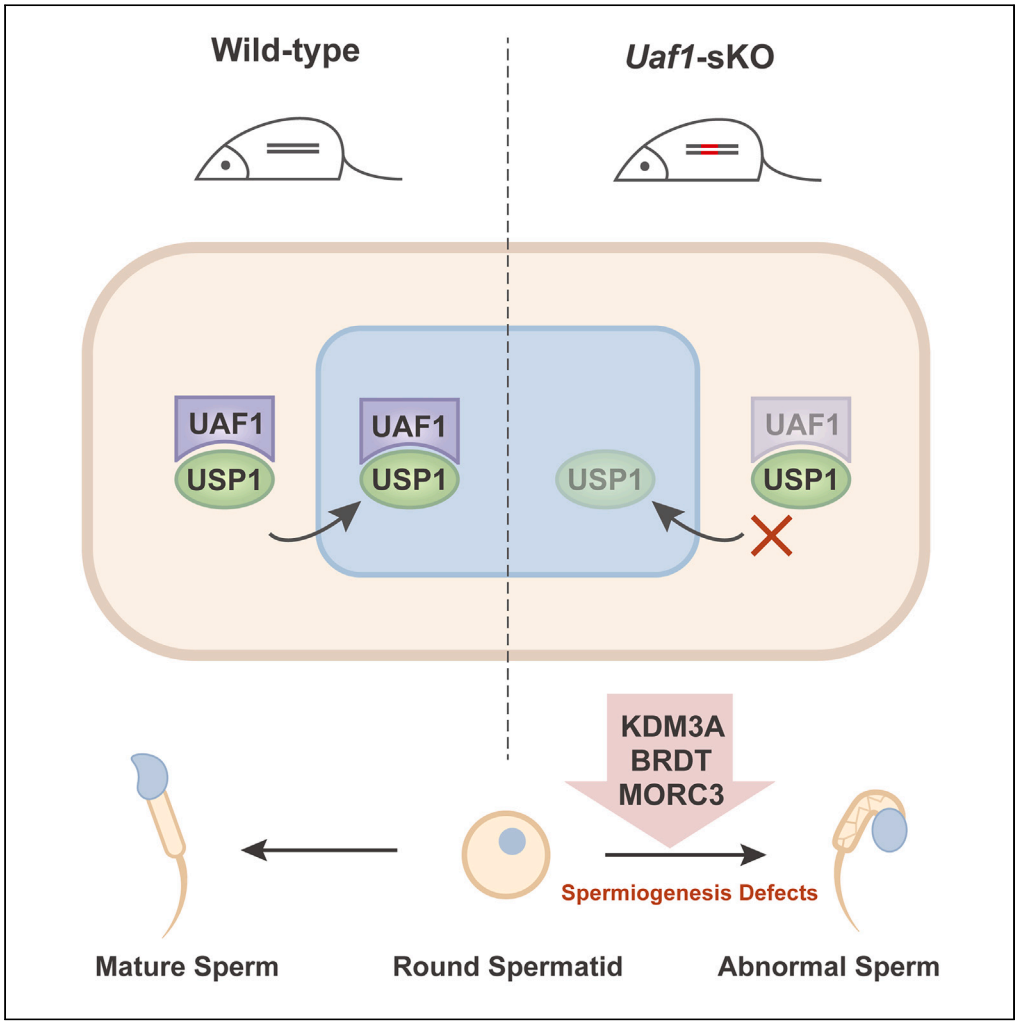

Ziqi Wang, Tongtong Li, Dongkai Liu, ..., Zi-Jiang Chen, Tao Huang, Hongbin Liu

chenzijiang@hotmail.com (Z.-J.C.)
htao1568@126.com (T.H.)
hongbin_sduivf@aliyun.com (H.L.)

Highlights

The germ cell-specific knockout of *Uaf1* impairs spermiogenesis, causing male infertility

UAF1 controls stabilization and subcellular localization of USP1 in testes

UAF1's role in regulating spermiogenesis proteins is essential for reproductive function

Wang et al., iScience 27, 109456
April 19, 2024
https://doi.org/10.1016/j.isci.2024.109456

iScience

CellPress
OPEN ACCESS

Article

The deubiquitinase cofactor UAF1 interacts with USP1 and plays an essential role in spermiogenesis

Ziqi Wang,[1,4,5,6] Tongtong Li,[1,4] Dongkai Liu,[1,4,5,6] Mengjing Li,[1,4,5,6] Shangming Liu,[11] Xiaochen Yu,[1,4,5,6] Hanzhen Li,[1,4] Hui Song,[7] Wei Zhao,[7] Zhaojian Liu,[8] Xiangfeng Chen,[9] Gang Lu,[1,2,10] Zi-Jiang Chen,[1,2,3,4,5,6,9,10,*] Tao Huang,[1,4,5,6,10,*] and Hongbin Liu[1,3,4,5,6,10,12,*]

SUMMARY

Spermiogenesis defines the final phase of male germ cell differentiation. While multiple deubiquitinating enzymes have been linked to spermiogenesis, the impacts of deubiquitination on spermiogenesis remain poorly characterized. Here, we investigated the function of UAF1 in mouse spermiogenesis. We selectively deleted *Uaf1* in premeiotic germ cells using the *Stra8-Cre* knock-in mouse strain (*Uaf1* sKO), and found that *Uaf1* is essential for spermiogenesis and male fertility. Further, UAF1 interacts and colocalizes with USP1 in the testes. Conditional knockout of *Uaf1* in testes results in disturbed protein levels and localization of USP1, suggesting that UAF1 regulates spermiogenesis through the function of the deubiquitinating enzyme USP1. Using tandem mass tag-based proteomics, we identified that conditional knockout of *Uaf1* in the testes results in reduced levels of proteins that are essential for spermiogenesis. Thus, we conclude that the UAF1/USP1 deubiquitinase complex is essential for normal spermiogenesis by regulating the levels of spermiogenesis-related proteins.

INTRODUCTION

Spermatogenesis is a complex morphogenetic differentiation process through which diploid spermatogonial stem cells are transformed into haploid spermatozoa in the seminiferous tubules of the testis. This differentiation process involves the self-renewal of spermatogonial stem cells, the differentiation of spermatogonia into meiotic spermatocytes, and morphogenesis of haploid spermatids referred to as spermiogenesis.[1] Spermiogenesis comprises five major processes, including: chromatin-remodeling, acrosome biogenesis, mitochondrial rearrangement, flagellum assembly, and cytoplasmic removal.[2] These differentiation processes are strictly regulated by transcriptional, translational, and post-translational mechanisms, and alterations in these processes result in male infertility and subfertility.[3] Spermiogenesis requires the precise temporal orchestration of multiple essential proteins, including KDM3A, BRDT, and MORC3. KDM3A plays an essential role in the regulation of sperm chromatin packaging and condensation by regulating the expression of transition nuclear protein 1 (TNP1) and protamine1 (PRM1).[4] BRDT binds to the hyperacetylated H4 tail and recognizes H4K5/K8ac through the BD1 domain, leading to the removal of histones in round spermatids.[5,6] MORC3, aMIWI2-associated partner, functions as an epigenetic regulator of piRNA-dependent transposon silencing in male germ cells.[7]

The level of a given protein in a cell depends on its rate of translation and degradation. Ubiquitination—one of the primary means through which cells regulate protein degradation—is mediated by ubiquitin-activating enzymes (E1s), ubiquitin-conjugating enzymes (E2s), and ubiquitin ligase enzymes (E3s).[8,9] In contrast, the removal of ubiquitin modifications from a substrate protein is mediated by deubiquitinating enzymes (DUBs).[10] In cells, the balance between ubiquitination and deubiquitylation activities regulates a wide variety of biological processes,

[1]Center for Reproductive Medicine, Shandong University, Jinan, Shandong 250012, China
[2]Shandong Key Laboratory of Reproductive Medicine, Shandong Provincial Hospital Affiliated to Shandong First Medical University, Jinan, Shandong, China
[3]Research Unit of Gametogenesis and Health of ART-Offspring, Chinese Academy of Medical Sciences, Jinan, Shandong 250012, China
[4]Key Laboratory of Reproductive Endocrinology of Ministry of Education, Shandong University, Jinan, Shandong 250012, China
[5]Shandong Provincial Clinical Medicine Research Center for Reproductive Health, Jinan, Shandong 250012, China
[6]Shandong Technology Innovation Center for Reproductive Health, Jinan, Shandong 250012, China
[7]Department of Immunology, Key Laboratory for Experimental Teratology of the Chinese Ministry of Education, School of Basic Medical Science, Cheeloo College of Medicine, Shandong University, Jinan, Shandong 250012, China
[8]Advanced Medical Research Institute, Shandong University, Jinan, China
[9]Shanghai Key Laboratory for Assisted Reproduction and Reproductive Genetics, Shanghai 200135, China
[10]CUHK-SDU Joint Laboratory on Reproductive Genetics, School of Biomedical Sciences, the Chinese University of Hong Kong, Hong Kong, China
[11]School of Basic Medical Sciences, Shandong University, Jinan 250012, China
[12]Lead contact
*Correspondence: chenzijiang@hotmail.com (Z.-J.C.), htao1568@126.com (T.H.), hongbin_sduivf@aliyun.com (H.L.)
https://doi.org/10.1016/j.isci.2024.109456

including various steps of spermatogenesis (e.g., maintenance/proliferation of the spermatogonia, meiotic entry, chromosomal recombination, acrosome biogenesis, and spermiogenesis).[11,12]

The more than 100 deubiquitinases encoded by the human genome are divided into six families. The ubiquitin-specific proteases (USPs) are the largest family,[13] and ubiquitin specific peptidase 1 (USP1) has been shown to deubiquitinate a wide range of substrates.[14–17] USP1 binds constitutively to an 80-kDa binding partner, referred to as USP1-associated factor 1 (UAF1, also called WDR48 or p80). Binding with UAF1 significantly enhances USP1's activity, by stabilizing its protein levels and mediating its access to substrates.[18–20] A previous study reported that *Uaf1*-deficient mice die during early embryonic development and that heterozygous inactivation of *Uaf1* results in gonadal dysfunction.[21] *Usp1*-deficient mice also exhibit perinatal lethality and impaired germ cell development.[22] However, the early death of *Uaf1*-deficient mouse embryos prevents the assessment of UAF1 function during later mammalian development and adult homeostasis. Thus, the potential roles of the UAF1-USP1 deubiquitinase complex in spermiogenesis remain unclear.

In this study, we found that the UAF1/USP1 deubiquitinase complex functions in regulating the levels of multiple spermiogenesis-related proteins. We found that UAF1 is present in the mouse testis and localizes to the nucleus in spermatids. We generated male mice with germ cell-specific *Uaf1* deletion mediated by Stra8-Cre (*Uaf1* sKO mice). *Uaf1* sKO male mice are completely infertile, have a significantly reduced number of epididymal sperm, and display defects in spermiogenesis. We show that UAF1 interacts and colocalizes with USP1 in testes. Conditional knockout of *Uaf1* in germ cells disrupts both the protein levels and localization of the deubiquitinating enzyme USP1, implicating altered ubiquitination in the observed spermiogenesis defects. Using proteomic approaches, we show that disrupting the function of the UAF1/USP1 deubiquitinase complex reduces the levels of multiple proteins with known functions in spermiogenesis in testes. Collectively, our results suggest that regulating the levels of multiple spermiogenesis-related proteins, the UAF1/USP1 deubiquitinase complex is essential for normal spermiogenesis.

RESULTS

UAF1 interacts with USP1 in mouse testes

UAF1 binds and stimulates three deubiquitinating enzyme complexes, including USP1, USP12, and USP46.[18,19] To determine which deubiquitinating enzyme binds to UAF1 in the testes, we performed immunoprecipitation followed by mass spectrometry of testicular protein extracts using an anti-UAF1 antibody. Our mass spectrometric analysis detected the presence of USP1 and USP12 in the purified UAF1 complex in mouse testes (Figure 1A). We next performed immunoprecipitation followed by mass spectrometry of testicular protein extracts using an anti-USP1 antibody and found that USP1 acts as a UAF1-interacting partner in mouse testes (Figure 1B). We verified the association of UAF1 and USP1 in testes by co-IP and immunoblotting, confirming (1) that USP1 was present among the immunoprecipitated proteins from wild-type (WT) testes using an anti-UAF1 antibody and (2) that UAF1 was present among the immunoprecipitated proteins from WT testes using an anti-USP1 antibody (Figures 1C and 1D). Additionally, we constructed an HA-tagged *Uaf1* knock-in mouse, and co-IP (co-immunoprecipitation) in UAF1-HA mice testes again showed an interaction between UAF1 and USP1 (Figure 1E). Collectively, these results indicate that UAF1 and USP1 form a deubiquitinase complex in the testes, which might participate in male spermatogenesis.

UAF1/USP1 displays a dynamic nuclear-cytoplasmic localization pattern during male spermatogenesis

Building upon our identification of UAF1 and USP1 interaction, we further analyzed their expression dynamics. Utilizing scRNA-seq data and UMAP visualization (Figure S1A), we discerned distinct cell clusters representing specific cell types such as A1, In, and RS7o8.[23] A concentrated examination of *Uaf1* and *Usp1* (Figure S1B) gene expression uncovered notably aligned expression trajectories. Both genes prominently manifested in a dense cluster situated in the upper left of the UMAP visualization, and exhibited a curvilinear path from the bottom left, stretching to the upper right. This alignment in expression was further bolstered by the violin plots (Figure S1C), which emphasized the variations in gene expression levels across multiple cell types. This congruence in spatial expression underscores a conceivable relationship between *Uaf1* and *Usp1*, potentially hinting at their synchronized roles during male spermatogenesis.

To explore the potential functions of UAF1 during mammalian male spermatogenesis, we initially examined the protein levels of UAF1 in mouse testes. Immunoblotting showed that UAF1 accumulates in various mouse organs, including ovaries and testes (Figure S2A). We also performed fractionation of testes extracts and found that UAF1 and USP1 were present in both the cytoplasmic and nuclear fractions as indicated by co-staining with β-Actin and Lamin B1 (Figure 2A). Germ cell development is strictly time-defined during embryonic and postnatal development in mouse testes.[24] We detected UAF1 in postnatal day 8 (PD8) testes, and found that the accumulation level increased throughout postnatal development and into adulthood (Figure 2B). These findings suggest that UAF1 may function in male spermatogenesis.

We subsequently performed immunofluorescence staining of paraffin sections of WT adult testes to evaluate the localization and distribution of the UAF1 protein during male spermatogenesis. Within the epithelium of the seminiferous tubules, spermatogenesis has been described as a sequence of 12 spatially synchronized stages (I–XII) along the length of the tubules, with a single stage being represented in one cross-section of the seminiferous tubules. The spermiogenesis process is further segregated into 16 steps (Sp.1–16) defined by the post meiotic morphologies of the spermatid acrosome and nucleus.[25–27] Interestingly, the co-staining against UAF1 and the acrosome marker PNA[28] revealed the presence of UAF1 throughout most stages of germ cell development, including in mitotic spermatogonia, meiotic spermatocytes, and early round spermatids (Figure 2C). We found that UAF1 was abundant in the cytoplasm of early stages of spermatocytes. UAF1 subsequently translocated to the nucleus of late stages of spermatocytes and round spermatids, with the highest protein levels detected in the nuclei of step 1–2 round spermatids (Figure 2D). Interestingly, double immunostaining revealed that UAF1 clearly colocalizes with USP1 in WT mice testes (Figure 2E). Further, we found that UAF1 and USP1 exhibited a similar dynamic translocation pattern between

A

Protein	MW (kDa)	# peptides
UAF1 (bait)	76	13
PHLPP1	182	6
USP1	87	2
USP12	43	2
WDR20	63	1

B

Protein	MW (kDa)	# peptides
USP1 (bait)	87	6
MORC3	107	7
UAF1	63	1

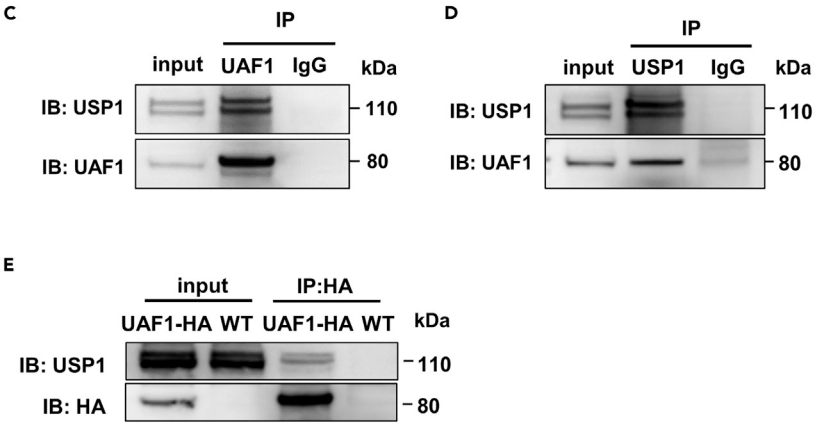

Figure 1. UAF1 interacts with USP1 in the testes

(A) Molecular weight (MW) and number of peptides detected by mass spectrometry for each of the indicated proteins that copurified with UAF1 from WT mouse testes.

(B) MW and number of peptides detected by mass spectrometry for each of the indicated proteins that copurified with USP1 from WT mouse testes.

(C and D) Co-IP analysis of UAF1 and USP1 from adult testicular protein extracts.

(E) Co-IP analysis of UAF1 and USP1 from UAF1-C-HA testicular protein extracts.

the nucleus and cytoplasm at different subtypes of male germ cells (Figures S3A and S3B). Subsequent immunoprecipitation assays using testicular extracts from PD3, PD6, and PD8 mice revealed that the interaction between UAF1 and USP1 begins before PD8 and becomes more pronounced by this stage. This pattern aligns with our immunofluorescence observations, providing further support that UAF1 and USP1 participate in a complex during male spermatogenesis (Figure S2D).

Additionally, immunofluorescence analyses of testes from HA-tagged *Uaf1* knock-in mice revealed the same pattern of UAF1 accumulation as observed in the WT animals with the anti-UAF1 antibody (Figure S2B). Further, we confirmed the nuclear localization of UAF1 and USP1 during meiotic prophase based on immunostaining of chromosome spreads (Figures S2C and S3C). These results collectively establish that UAF1 and USP1 exhibit dynamic nuclear-cytoplasmic translocation patterns in male germ cells postnatally, and may be involved in male spermatogenesis.

UAF1 is essential for male fertility

To elucidate the physiological functions of UAF1 during male spermatogenesis, we used a conditional knockout approach in which a *Uaf1* floxed line (*Uaf1*$^{fl/fl}$, in which exons 2 and 4 of the *Uaf1* allele are flanked by *loxP* sites)[17] was crossed with *Stra8-Cre* knock-in mice[29] expressing CRE recombinase in male germ cells from PD3 (i.e., before they initiate meiosis) (Figure 3A). Immunoblotting indicated that the protein level of UAF1 was dramatically reduced in the testes of *Uaf1* sKO male mice compared with WT (Figure 3B). Further, immunofluorescence staining indicated that UAF1 was absent from *Uaf1* sKO male germ cells (Figure 3C). These results indicated that UAF1 was successfully deleted in male germ cells.

The *Uaf1* sKO male mice were viable and appeared normal; however, a 5-month fecundity test showed that they were completely infertile (Figure 3D). Consistent with this infertile phenotype, the testis size of *Uaf1* sKO mice was significantly smaller than WT, by ~50% (Figures 3E and 3F), and the testis-to-body weight ratio was significantly decreased as compared with WT (Figures 3G and 3H). In contrast to males, the fertility of *Uaf1* sKO females was normal (Figures S4A and S4B). Morphological analysis at 3 and 6 months showed that the *Uaf1* sKO ovaries exhibited normal ovarian morphology (Figure S4C). Co-IP in the ovary confirmed the interaction between UAF1 and USP1 in WT ovaries (Figure S4D). Immunofluorescence analysis showed that UAF1 and USP1 exhibit uniformly distributed localization patterns in the ovaries (Figure S4E). Notably, UAF1 is primarily localized in oocytes and granulosa cells. Thus, conditional knockout of *Uaf1* results in spermatogenesis

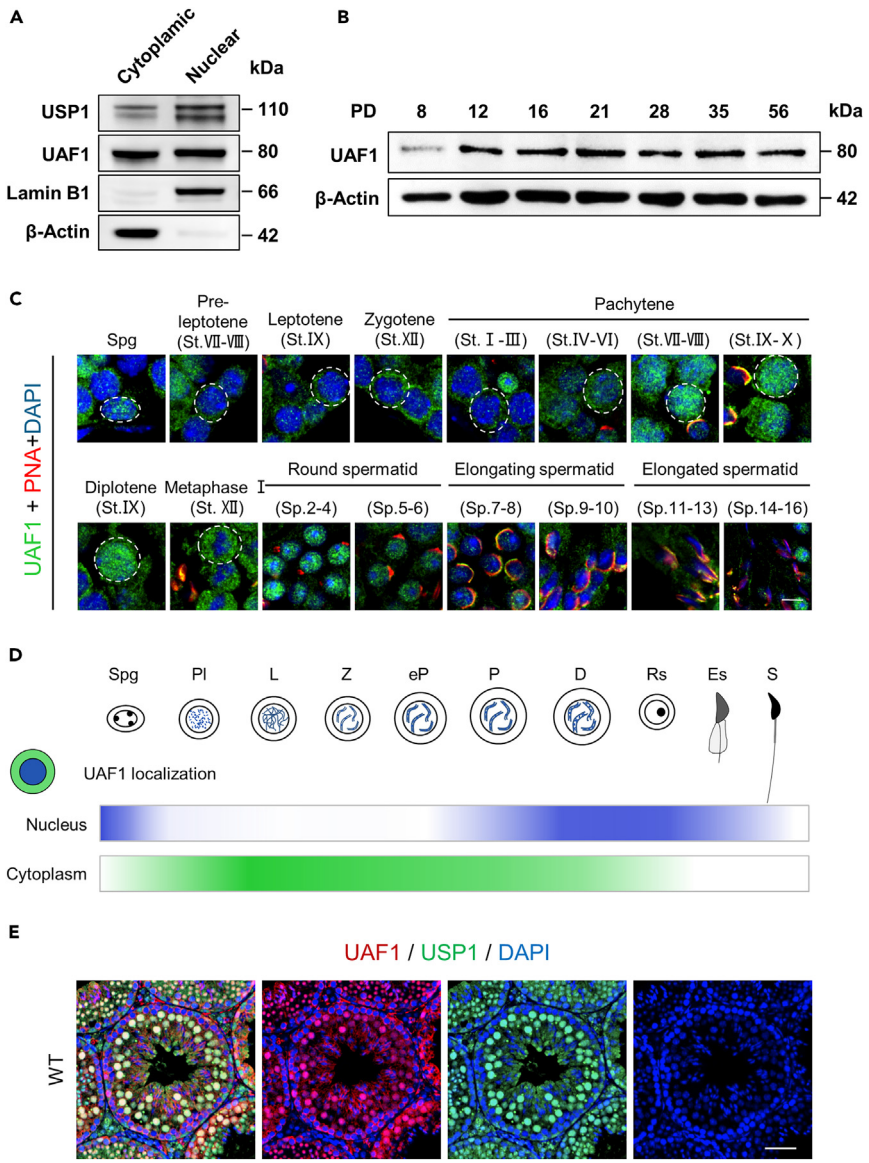

Figure 2. UAF1 protein levels and dynamic localization in the testes

(A) Western blotting of UAF1 and USP1 in cytoplasmic and nuclear fractions from adult WT testes, showing that UAF1 and USP1 are present in the cytoplasm and in nuclei. Lamin B1 was used as the marker for the nuclear fraction, and β-Actin was used as the marker for the cytoplasmic fraction.

(B) UAF1 was detected starting in PD8 testes. β-Actin served as a loading control.

(C) Double immunostaining against UAF1 and PNA in WT germ cells from testis sections of the indicated stages, showing UAF1's dynamic localization pattern during adult spermatogenesis. DNA was counterstained with DAPI. Scale bar, 5μm.

(D) A schematic summary of UAF1 localization in adult testis during spermatogenesis. Spg, Spermatogonia; Pl, preleptotene; L, leptotene; Z, zygotene; eP, early pachytene; P, pachytene; D, diplotene; Rs, round spermatids; Es, elongating spermatids; S, Spermatozoa.

(E) Immunofluorescence staining against the UAF1 (red) and USP1 (green) in testes of 12-week-old WT mice. Scale bar, 50 μm.

defects and infertility in males but does not affect female fertility, suggesting a sexually dimorphic function of UAF1 in male and female fertility.

Haploid germ cell development is defective in *Uaf1* sKO mice

To further explore the function of UAF1 in male spermatogenesis, we next performed hematoxylin staining of testis sections from 12-week-old WT and *Uaf1* sKO mice. WT testes had normal spermatogenesis and elongated spermatids in almost all tubules, whereas testes from adult *Uaf1* sKO mice exhibited a decrease in the diameter of the seminiferous tubules and a reduced number of germ cells (Figure 4A). Notably, we

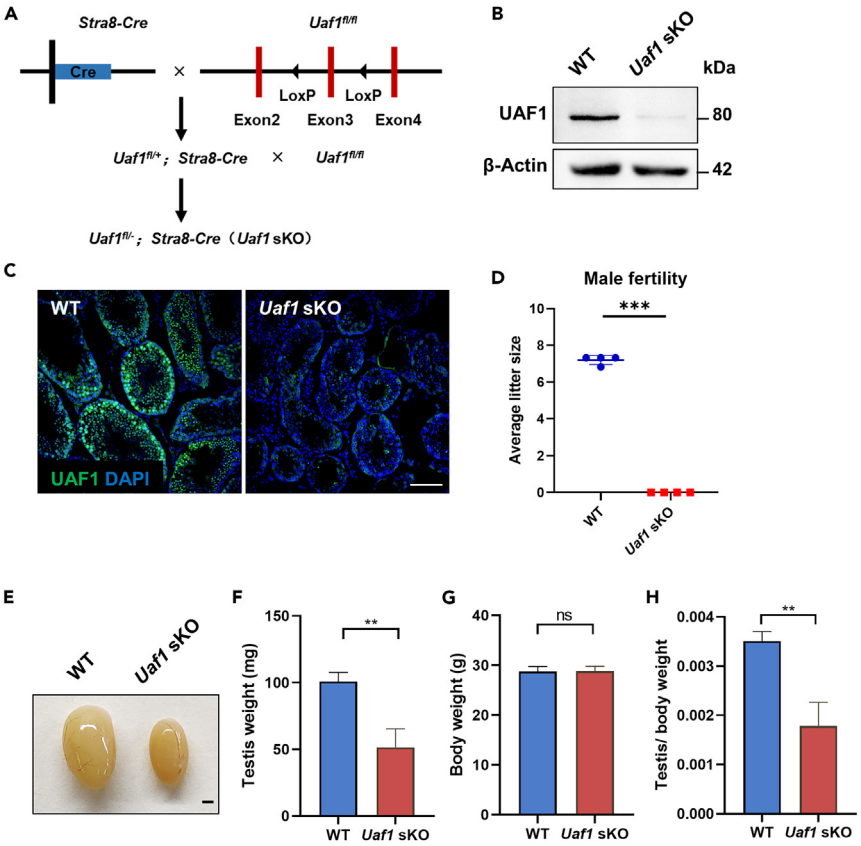

Figure 3. Conditional knockout of *Uaf1* in germ cells results in reduced testicular size and male infertility

(A) Hybrid approach used to generate the *Uaf1* sKO mice with *Uaf1* specifically deleted in germ cells.

(B) Western blotting against UAF1 in testes from 8-week-old WT and *Uaf1* sKO testes (n = 3). β-Actin served as the loading control.

(C) UAF1 immunofluorescence in WT and *Uaf1* sKO adult testis. Scale bar, 100 μm.

(D) Number of pups per litter from male mice (>8-week-old) naturally crossed with WT female mice for 6 months. *Uaf1* sKO male mice were completely infertile. Data are presented as the mean ± SEM, n = 4. ***p < 0.001 by Student's *t* test.

(E) Gross morphology of representative testes from WT and *Uaf1* sKO mice. Scale bar, 1 mm.

(F) Weights of testes from *Uaf1* sKO and age-matched control mice. Data presented as mean ± SEM, n = 3. **p < 0.01 by Student's *t* test.

(G) Body weights from *Uaf1* sKO and age-matched control mice. n = 3. n.s., no statistical significance.

(H) Quantification ratio of testis weight/body weight in *Uaf1* sKO and age-matched control mice. Data presented as mean ± SEM, n = 3. **p < 0.01 by Student's *t* test.

detected no change in the numbers of tubules per testis cross-section or in the number of Sertoli cells per tubule cross-section (Figures S4F–S4G). Immunofluorescence staining of testes sections against the germ cell-specific marker MVH indicated germ cell loss in *Uaf1* sKO testes (Figures 4B and S4H).

We subsequently performed immunofluorescence staining of seminiferous tubule sections of adult testes with the meiotic synapsis marker SYCP3, which indicated that the testicular seminiferous tubules of adult *Uaf1* sKO mice entered meiosis (Figure S5A). We found that the number of meiotic cells in the *Uaf1* sKO mice was significantly decreased compared with WT mice (Figure S5B). Further, spermatocytes of *Uaf1* sKO were analyzed by chromosome spreading with SYCP1, SYCP3, γH2AX, and MLH1 staining (Figures S5C–S5E), and we found that *Uaf1* sKO had typical numbers of leptotene, zygotene, pachytene and diplotene meiotic cells. There was no obvious difference between WT and *Uaf1* sKO spermatocytes. The induction of meiotic synapsis (marked by SYCP1), DSB repair (marked by γH2AX), and crossover events (marked by MLH1) were unaffected. These observations showed that the defects in spermatogenesis observed in *Uaf1* sKO male mice occurred after meiosis.

We next used PAS–hematoxylin staining to assess post meiotic development in *Uaf1* sKO testes (Figure 4C). We found that round spermatids and early elongating spermatids were unaltered in the seminiferous tubules of *Uaf1* sKO testes. However, late spermatid development was compromised in *Uaf1* sKO testes, and fewer condensing spermatids were identified (stages I, II–III) and the number of condensed mature spermatids was drastically reduced (stages IV–VI, VII–VIII), concomitant with the apoptotic signals detected in late spermatids (Figures 4D and 4E). By examining the histology of *Uaf1* sKO and WT testes at various developmental time points (PD24, 28, 32, and 45), we found that *Uaf1* sKO testes contained aberrant seminiferous tubules and delayed round spermatid development at PD28 and beyond. Upon deletion of *Uaf1* in the testes, germ cells were gradually lost starting from PD28, and the onset of the first wave of germ cell development was markedly delayed in *Uaf1* sKO testes (Figure S6A). These results demonstrated that haploid germ cell development was defective in *Uaf1* sKO mice.

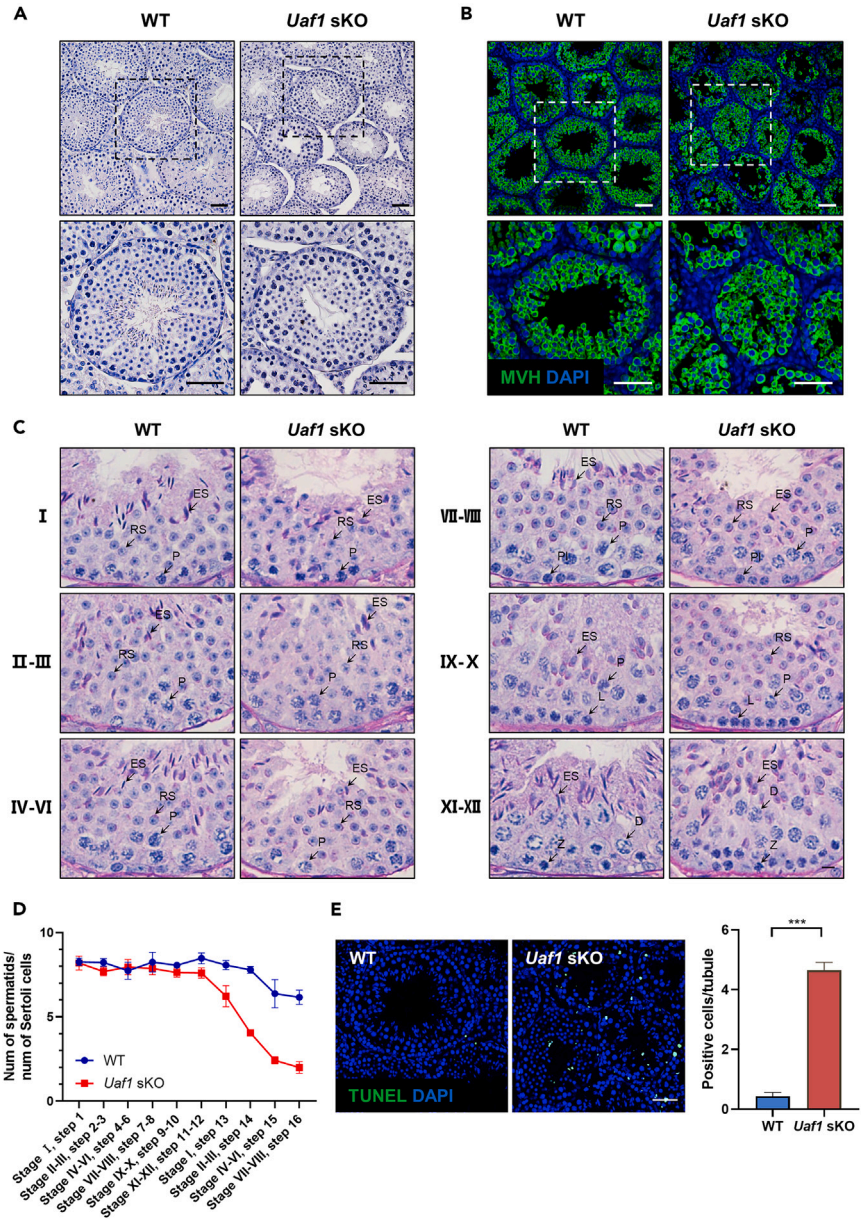

Figure 4. Spermiogenesis is defective in *Uaf1* sKO mice

(A) Hematoxylin staining of histological sections of the testes prepared from 12-week-old WT and *Uaf1* sKO mice. Scale bar, 50 μm.

(B) Immunofluorescence staining against the mouse VASA homolog (MVH) in testes of 12-week-old WT and *Uaf1* sKO mice. Scale bar: 50 μm.

(C) PAS-hematoxylin staining of testis sections from 12-week-old WT and *Uaf1* sKO mice. Stages of seminiferous epithelium cycles were determined by morphology of spermatocytes and round spermatids. Pl, preleptotene; L, leptotene; Z, zygotene; P, pachytene; D, diplotene; RS, round spermatids; ES, elongating spermatids. Scale bar, 20 μm.

(D) Ratios of the numbers of spermatids to Sertoli cells in tubule cross sections of specific stages of seminiferous epithelial cycles and the corresponding steps of spermatid development are shown. There was a reduced number of late spermatids in *Uaf1* sKO testes.

(E) Left: TUNEL assays of testis sections from 12-week-old WT and *Uaf1* sKO mice. Scale bar, 50 μm. Right: Quantification of the numbers of TUNEL-positive cells per tubule. Data are presented as the mean ± SEM, n = 3. ***$p < 0.001$ by Student's *t* test.

Spermiogenesis is defective in *Uaf1* sKO mice

We subsequently dissected the epididymis and examined the mature sperm. We consistently found that there were only a few spermatozoa in the epididymal lumen of *Uaf1* sKO male mice. We also observed an accumulation of immature germ cells and aberrant sperm in the cauda epididymis of *Uaf1* sKO mice (Figure 5A). We examined the spermatozoa released from the caudal epididymis and found the sperm count in

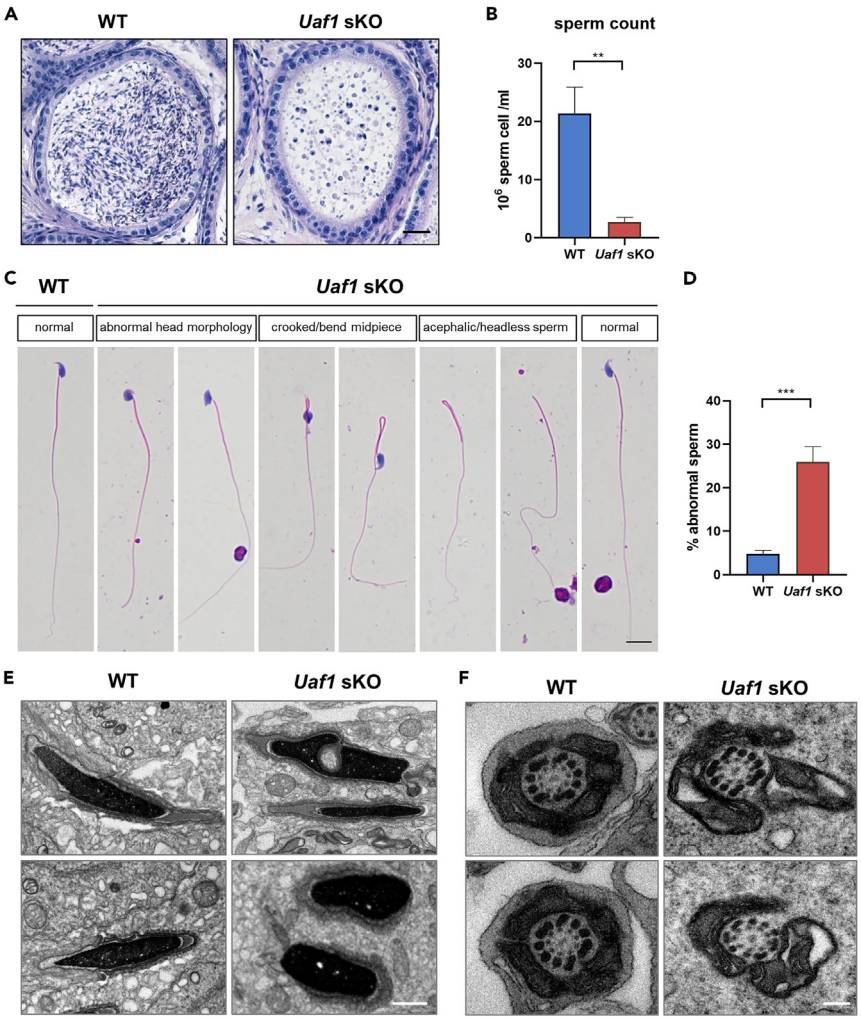

Figure 5. The late steps of spermatid development are disrupted in *Uaf1* sKO testes

(A) Hematoxylin staining of histological sections of the cauda epididymis prepared from 12-week-old WT and *Uaf1* sKO mice. Scale bar, 20 μm.

(B) Sperm counts in cauda epididymis from 12-week-old WT and *Uaf1* sKO mice. Data presented as mean ± SEM, n = 3. **p < 0.01 by Student's *t* test.

(C) Hematoxylin and eosin staining of sperm from 12-week-old WT and *Uaf1* sKO mice. Scale bar, 10 μm. Note that the majority of sperm exhibited deformed head morphology in the *Uaf1* sKO cauda epididymis.

(D) Spermatocytograms showing the number of abnormal sperms in WT and *Uaf1* sKO mice. Data are presented as the mean ± SEM, n = 3. ***p < 0.001 by Student's *t* test.

(E) Representative transmission electron micrographs of sperm heads from dpp 12-week-old WT and *Uaf1* sKO mice. Scale bar, 1 μm.

(F) Representative transmission electron micrographs of sperm cross-section ultrastructure from dpp 12-week-old WT and *Uaf1* sKO mice. Scale bar, 2 μm.

the *Uaf1* sKO mice to be significantly decreased compared with WT mice (Figure 5B). To determine the morphological characteristics of the spermatozoa, single spermatozoon analysis by HE staining was performed and the results indicated that *Uaf1* sKO sperm had numerous anomalies, including abnormal head formation, acephalic/headless sperm, and sperm with a bent midpiece (Figure 5C). The ratio of *Uaf1* sKO spermatozoa with abnormal heads and flagella was significantly increased compared with WT (Figure 5D). Indeed, transmission electron microscopy (TEM) inspection of sperm further confirmed that the *Uaf1* sKO sperm heads showed morphological abnormalities (Figure 5E). We also observed aberrant mitochondrial arrangement in *Uaf1* sKO spermatids (Figure 5F). TEM of sperm from WT and *Uaf1* sKO mice revealed no structural abnormalities in axoneme organization or the fibrous sheath in *Uaf1* sKO mice (Figure S7A). Given that the *Uaf1* sKO mice still produced some sperm, we used computation-assisted semen analyses (CASA) to characterize these sperm. The sperm from *Uaf1* sKO mice displayed little movement or forward progression (Figure S7B); thus, beyond the observed reduction in sperm number, the functionality of *Uaf1* sKO sperm was also compromised. The irregularly shaped sperm heads, reduced sperm count, and reduced sperm motility, together, account for the infertility phenotype observed in *Uaf1* sKO males. Collectively, these observations suggested that the infertility of *Uaf1* sKO male mice was likely due to defects in the post-meiotic stages of male spermatogenesis, known as spermiogenesis.

UAF1 controls the stabilization and subcellular localization of USP1 in testes

Previous reports show that USP1 and UAF1 form a complex and function together, and UAF1 significantly enhances USP1 activity by stabilizing its protein levels and mediating its access to substrates.[14,20] USP1 and UAF1 form a complex in the cytoplasm that is subsequently translocated to the nucleus through active nuclear import mediated by the two USP1 NLSs.[30] In this study, we found that UAF1 and USP1 form a deubiquitinase complex in testes. UAF1 exhibits a dynamic nuclear-cytoplasmic translocation pattern during spermatogenesis. Likewise, USP1 has been shown to have a similar dynamic translocation pattern between the cytoplasm and nuclei at different subtypes of male germ cells. Collectively, we found that UAF1 interacts and colocalizes with USP1 in the testes.

To investigate whether UAF1 regulates spermiogenesis through USP1, we performed immunostaining and immunofluorescence of USP1 in *Uaf1* sKO male testes. We found that the levels of USP1 were substantially reduced, and there was a marked decrease in full-length USP1 and an almost complete loss of the N-terminal USP1 cleavage product in testes from *Uaf1* sKO male mice as compared with WT, which indicated that stabilization of USP1 is regulated by UAF1 (Figure S8A). To investigate the influence of UAF1 on the subcellular distribution of USP1 in the testis, we examined USP1 localization in *Uaf1* sKO and WT spermatids at different developmental stages (Figure S8B). Interestingly, we observed that USP1 is more abundant in the cytoplasm of *Uaf1* sKO round spermatids than in WT. These results revealed that UAF1 is required for USP1 stabilization and subcellular localization during spermatogenesis, and UAF1 may regulate spermiogenesis through the deubiquitinase function of USP1.

The levels of spermiogenesis-related proteins are altered in *Uaf1* sKO mice testes

Spermiogenesis is a complex developmental process that is affected by the regulation of gene transcription and translation and by targeted protein degradation.[31] Previous studies have shown that spermatogenesis is dependent on the balance between ubiquitination and deubiquitination.[11,12] To understand the protein changes occurring during spermiogenesis in the *Uaf1* sKO testes, round spermatids were isolated from WT and *Uaf1* sKO testes using fluorescence-activated cell sorting (FACS) and then subjected to quantitative TMT based proteomics.

A total of 684 proteins with differential abundance (with a 1.3-fold change cutoff) were identified in the testes of *Uaf1* sKO mice compared to WT mice, of which 303 showed decreased abundance while 381 showed increased abundance (Figures 6A–6C; Table S2). Gene ontology analysis identified functional enrichment for terms such as "protein-DNA complex assembly", "spermiogenesis", and "histone modification", among others (Figure 6D). Based on previous knockout studies reporting impaired male fertility,[4–7] we focused on three proteins (KDM3A, BRDT, MORC3). Using the Power Law Global Error Model (PLGEM), we analyzed identified proteins, and quantified 670 differentially expressed proteins with a p value threshold of less than 0.01 (Tables S3, S4, and S5). We established a fold change threshold of 1.5 and determined that KDM3A, BRDT, and MORC3 are consistently categorized within the down-regulated subset (Figures S9A–S9C). Immunoblotting indicated that the levels of KDM3A, BRDT, and MORC3 were substantially reduced in round spermatids from *Uaf1* sKO male mice as compared with WT. These results suggest that UAF1 is a regulator of normal reproductive functioning via its regulation of multiple proteins involved in spermiogenesis.

DISCUSSION

Here, we show that the deubiquitinating enzyme cofactor UAF1 is specifically required for spermiogenesis in male mice. *Uaf1* sKO male mice are completely infertile because haploid germ cell development is defective, which is accompanied by abnormal sperm morphology and function. Consistent with previous studies, we found that UAF1 interacts and colocalizes with USP1 in the testes, suggesting an interplay between UAF1 and USP1 in spermiogenesis. Loss of UAF1 led to altered protein levels and localization of USP1 in the testes. Additionally, conditional knockout of *Uaf1* in testes resulted in reduced levels of proteins essential for spermiogenesis. We conclude that UAF1 is indispensable for regulating the levels of multiple spermiogenesis-related proteins, thus making it essential for normal spermiogenesis.

Spermatogenesis relies on the proper function and subcellular localization of several UPS enzymes, and disruption of DUB genes can cause male infertility and spermatogenic disorders.[12] Several DUBs, such as USP2, USP7, USP8, USP9Y, USP9X, USP14, USP26, USP42, UCH-L1, UCH-L3, UCH-L4, UCH-L5, and CYLD, have been implicated in spermatogenesis.[31,32] However, little research has been conducted on the role of DUB cofactors in this process. The WD-40 domain plays an important role in the ubiquitin-proteasome system, with over twenty WD-40-related USPs associated with various cellular processes.[33] USP1/UAF1, a typical USP/WD40 complex, has been extensively studied. Our findings show that UAF1, a scaffold protein essential for the activity of ubiquitin-specific peptidases, interacts with USP1 and is involved in spermiogenesis.

We observed that UAF1 and USP1 interact in the ovary. Immunofluorescence analysis revealed their widespread distribution within the ovary, with significant co-localization in granulosa cells. This suggests a potential functional role for UAF1 and USP1 in granulosa cells. Despite the conditional knockout of *Uaf1* in mice using *Stra8-Cre*, female fertility remained unaffected. These findings imply that UAF1's role varies between males and females. It raises the possibility that a targeted knockout of *Uaf1* in granulosa cells might lead to infertility in female mice, which could provide further insights into UAF1's specific functions in female reproductive biology.

UAF1 acts as a cofactor for USP1, USP12, and USP46, enhancing their deubiquitinase activity by forming stable UAF1/USP protein complexes.[14,18] Defective spermiogenesis in *Uaf1 sKO* mice necessitated the identification of a DUB critical for this process. Mass spectrometry analysis revealed the presence of USP1 and USP12 along with the purified UAF1 complex, suggesting that UAF1 may also act as a cofactor for USP1 and USP12 in the testes. USP1, a well-known deubiquitinase essential in maintaining cellular homeostasis and responding to DNA damage, has been found to participate in diverse cellular processes according to previous studies.[34–36] In *Usp1*-deficient mice, seminiferous tubules displayed significant atrophy and were mostly devoid of spermatogenic cells.[22] In this study, we demonstrated that UAF1 interacts and colocalizes with USP1 in the testes, thus exhibiting a similar dynamic pattern of cytoplasmic-nuclear translocation during spermatogenesis,

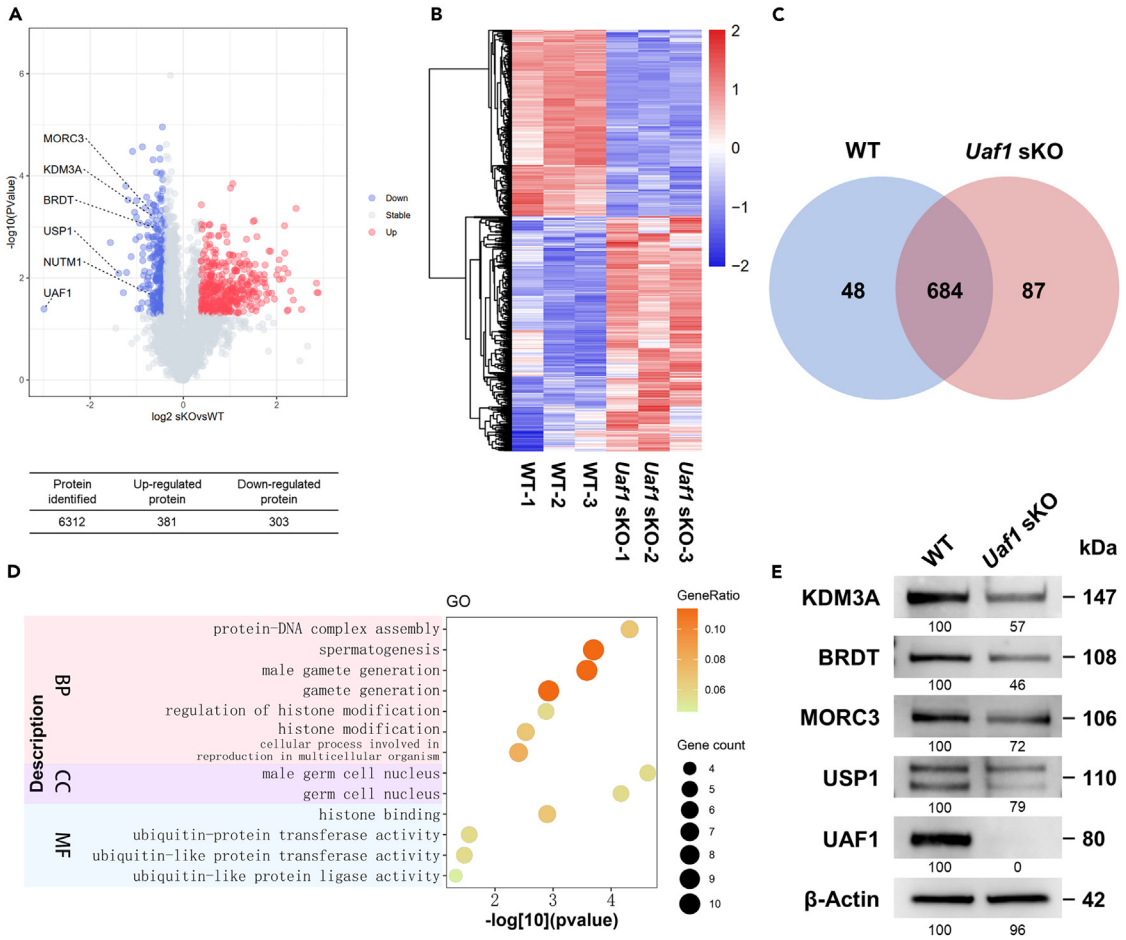

Figure 6. Proteomic analyses of round spermatids from WT and *Uaf1* sKO mice

(A) Volcano plot of protein levels between WT and *Uaf1* sKO round spermatids. Average protein abundance ratio of 3 replicates (log 2 transformed) between 8-week-old WT and *Uaf1* sKO mice round spermatids, plotted against the p value by t-test (−log 10 transformed). The criteria for determining differential protein abundance were set at a p value of ≤0.05 and 1.3-fold change in either WT or *Uaf1* sKO round spermatids. The table shows the total number of proteins identified, as well as the number of up- and down-regulated proteins. The detailed information on protein groups is listed in Table S2.

(B) Heatmap displaying the abundance of 6312 proteins that differed expressed between WT and *Uaf1* sKO round spermatids. The proteins were chosen based on the following criteria: fold change ≥1.3 and a q-value <0.05.

(C) Venn diagram indicating the overlap of proteins with altered abundance identified and quantified in WT and *Uaf1* sKO round spermatids.

(D) GO analysis of the significantly changed proteins identified in biological processes, molecular function, and cellular components.

(E) The protein levels of KDM3A, BRDT, and MORC in testes from WT and *Uaf1* sKO mice (n = 3). β-Actin served as the loading control.

and the translocation of UAF1/USP1 from the cytoplasm to the nucleus between mid-pachytene and round spermatids appears to be essential for proper spermiogenesis. USP1 is stabilized and activated by UAF1 *in vivo* and *in vitro*.[14] Previous studies have shown that USP1 and UAF1 form a complex in the cytoplasm that is subsequently translocated to the nucleus through active nuclear import mediated by the two USP1 NLSs.[30] Conditional knockout of *Uaf1* in the testes results in reduced activity and impaired nuclear-cytoplasmic translocation in round spermatids, thus compromising their function. These defects likely underlie the spermiogenesis abnormalities observed in *Uaf1* sKO mice. However, our current lack of an effective USP12 antibody prevents us from determining whether UAF1 affects USP12 binding and/or any associated deubiquitinating enzyme activity in testes.

Our mass spectrometric analysis detected the presence of PHLPP1 and WDR20 in the purified UAF1 complex in mouse testes. PHLPP1 is crucial in HPV DNA replication through its interaction with UAF1 in the E1 helicase.[37] Additionally, its association with WDR48 and USP12 suggests a potential tumor-suppressive role.[38] UAF1 interacts with USP1, USP12, and USP46, but the activation mechanism involving WDR20 differs among them.[39–41]Collectively, these observations highlight the intricate regulatory dynamics between UAF1, WDR20, and USPs, emphasizing the need for a deeper exploration of their broader cellular implications.

Uaf1 sKO mice showed reduction in meiotic cells, but important meiotic processes such as meiotic synapsis, DSB repair, and crossover events remained unaffected. The presence of a large number of haploid spermatids in the seminiferous tubules of *Uaf1* sKO mice suggests

the onset of phenotypic alterations post-meiotic. We hypothesize that the conditional knockout of *Uaf1* in testes leads to these phenotypic changes rather than a meiotic defect because UAF1 affects downstream molecules in a quantitative rather than qualitative manner.

Building upon previous research, we further probed the interplay between UAF1 and the classical downstream molecules, FANCD2 and PCNA.[14,42] Through immunofluorescence staining of testes sections, we observed a reduction in FANCD2 and PCNA (Figures S10A and S10B). This reduction paralleled the germ cell loss noted in *Uaf1* sKO testes (Figures S10C and S10D). It is essential to emphasize that this observed reduction in the protein levels of FANCD2 and PCNA in the whole testicular tissue of *Uaf1* sKO mice (Figure S10E) might be more reflective of the altered cell composition between WT and *Uaf1* sKO, rather than a direct regulatory impact of UAF1 on these proteins. Previous studies on *Fancd2* and *Pcna* knockout mice exhibited impaired spermatogenesis.[43,44] These results suggest that the conditional knockout of *Uaf1* might impact the overall testicular cell composition, leading to apparent differences in protein levels of FANCD2 and PCNA, rather than a direct regulatory role on these proteins. Still, it is essential to emphasize that, even in the presence of these altered protein levels, a significant cell population progressed to the round spermatid phase. However, potential diminished cellular functionality combined with effects from other molecules could have led to the observed post-meiotic apoptosis in these cells.

The function of UAF1 in spermiogenesis was investigated in round spermatids using a proteomics approach to elucidate the potential mechanism behind UAF1's involvement in male infertility. The results showed that *Uaf1* sKO mice had significantly reduced levels of proteins that are critical for sperm production and fertilization. Further, bioinformatics analysis and a literature review also revealed that essential proteins, which are recently shown to cause impaired male fertility, were considerably downregulated. Notably, our research includes genes whose knockouts are linked to meiosis impairment in mice, such as *Arid2* and *Mdc1*[45,46]; genes associated with disrupted spermatogenesis following knockout, like *Brd7* and *Fndc3a*[47,48]; and genes that, upon knockout, lead to acrosomal abnormalities, including *Sirt1* and *Kiaa0319L*.[49,50] We theorize that the diminishment of these proteins contributes to the impaired spermatogenesis observed in conditional knockout of *Uaf1* in testes. The impact of UAF1 on downstream proteins is more about quantity than quality, making the phenotype of its conditional knockout in testes complex and diverse. To further investigate this, we have selected KDM3A, BRDT, and MORC3 for validation, based on their phenotypic similarities to the effects seen in *Uaf1* sKO. Deletion of lysine-specific demethylase 3A (*Kdm3a*) is the most well-known cause of post-meiotic chromatin condensation defects,[4] and *Brdt* ΔBD1 mice exhibit impaired binding to H4K5/K8ac, which results in the failure of histone removal.[5,6] Additionally, conditional knockout of *Morc3* in the testes leads to subfertility in male mice.[7] Overall, our findings reveal that KDM3A, BRDT, and MORC3 are potential mediators of the spermiogenesis impairments observed in *Uaf1* sKO testes.

In summary, we have pinpointed UAF1 as a deubiquitinating enzyme cofactor that is indispensable in guiding spermiogenesis in male mice. Further investigations into the complex formation of UAF1 and USP1 within the testes, and the regulation of multiple proteins involved in spermiogenesis by UAF1, will be of great importance in understanding the regulation of deubiquitylation in mammalian spermiogenesis.

Limitations of the study

In this study, we explored the phenotypic and molecular effects of the conditional knockout of *Uaf1* in testes and its significance in spermiogenesis and male fertility using the *Stra8-Cre* knock-in mouse model (*Uaf1* sKO). We observed an interaction and colocalization between UAF1 and USP1 in the testes. Through tandem mass tag-based proteomics, proteins with altered abundance were identified in *Uaf1* sKO, suggesting the role of the UAF1/USP1 deubiquitinase complex in spermiogenesis. However, while we detailed the relationship between UAF1 and USP1, it remains uncertain if UAF1 interacts in a similar manner with other USP molecules. Further, this study primarily addresses the effects of UAF1 after the initiation of meiosis. The potential role of UAF1 in spermatogonial stem cell maintenance or during the PGC stage has not been covered and warrants further investigation.

STAR★METHODS

Detailed methods are provided in the online version of this paper and include the following:

- KEY RESOURCES TABLE
- RESOURCE AVAILABILITY
  - Lead contact
  - Materials availability
  - Data and code availability
- EXPERIMENTAL MODEL AND STUDY PARTICIPANT DETAILS
- METHOD DETAILS
  - Histology, immunostaining, TEM, TUNEL assay
  - CASA
  - Western blotting
  - Immunoprecipitation
  - Fluorescence-activated cell sorting of round spermatids
  - Proteomic analysis
- QUANTIFICATION AND STATISTICAL ANALYSIS
  - Bioinformatics analysis
  - Statistical analyses

SUPPLEMENTAL INFORMATION

Supplemental information can be found online at https://doi.org/10.1016/j.isci.2024.109456.

ACKNOWLEDGMENTS

We thank all our colleagues in the Chen laboratory for helpful discussions. We appreciate the support of the Translational Medicine Core Facility of Shandong University for consultation and instrument use. Funding: National Key R&D Program of China [2021YFC2700200, 2021YFC2700600]; Research Unit of Gametogenesis and Health of ART-Offspring, Chinese Academy of Medical Sciences [2020RU001]; Academic Promotion Programme of Shandong First Medical University [2019U001]; Major Innovation Projects in Shandong Province [2021ZDSYS16]; Science Foundation for Distinguished Young Scholars of Shandong [ZR2021JQ27]; Taishan Scholars Program for Young Experts of Shandong Province [tsqn202103192]; Basic Science Center Program of NSFC [31988101]; Shandong Provincial Key Research and Development Program [2020ZLYS02].

AUTHOR CONTRIBUTIONS

H.B.L. and T.H. conceived and designed the entire project. Z.W. performed most of the experiments. Z.W. and T.L. were responsible for analyzing the proteomic data. Z.-J.C. and H.B.L. supervised the whole project. Z.W. and T.H. analyzed the data and wrote the manuscript with the assistance of the other authors. All authors read and approved the final paper.

DECLARATION OF INTERESTS

The authors declare no competing interests.

Received: April 2, 2023
Revised: August 2, 2023
Accepted: March 7, 2024
Published: March 11, 2024

REFERENCES

1. Hess, R.A., and Renato de Franca, L. (2008). Spermatogenesis and cycle of the seminiferous epithelium. Adv. Exp. Med. Biol. *636*, 1–15. https://doi.org/10.1007/978-0-387-09597-4_1.
2. Zhou, J., Yang, F., Leu, N.A., and Wang, P.J. (2012). MNS1 is essential for spermiogenesis and motile ciliary functions in mice. PLoS Genet. *8*, e1002516. https://doi.org/10.1371/journal.pgen.1002516.
3. Neto, F.T.L., Bach, P.V., Najari, B.B., Li, P.S., and Goldstein, M. (2016). Spermatogenesis in humans and its affecting factors. Semin. Cell Dev. Biol. *59*, 10–26. https://doi.org/10.1016/j.semcdb.2016.04.009.
4. Okada, Y., Scott, G., Ray, M.K., Mishina, Y., and Zhang, Y. (2007). Histone demethylase JHDM2A is critical for Tnp1 and Prm1 transcription and spermatogenesis. Nature *450*, 119–123. https://doi.org/10.1038/nature06236.
5. Gaucher, J., Boussouar, F., Montellier, E., Curtet, S., Buchou, T., Bertrand, S., Hery, P., Jounier, S., Depaux, A., Vitte, A.L., et al. (2012). Bromodomain-dependent stage-specific male genome programming by Brdt. EMBO J. *31*, 3809–3820. https://doi.org/10.1038/emboj.2012.233.
6. Shang, E., Nickerson, H.D., Wen, D., Wang, X., and Wolgemuth, D.J. (2007). The first bromodomain of Brdt, a testis-specific member of the BET sub-family of double-bromodomain-containing proteins, is essential for male germ cell differentiation. Development *134*, 3507–3515. https://doi.org/10.1242/dev.004481.
7. Kojima-Kita, K., Kuramochi-Miyagawa, S., Nakayama, M., Miyata, H., Jacobsen, S.E., Ikawa, M., Koseki, H., and Nakano, T. (2021). MORC3, a novel MIWI2 association partner, as an epigenetic regulator of piRNA dependent transposon silencing in male germ cells. Sci. Rep. *11*, 20472. https://doi.org/10.1038/s41598-021-98940-7.
8. Hermo, L., Pelletier, R.M., Cyr, D.G., and Smith, C.E. (2010). Surfing the wave, cycle, life history, and genes/proteins expressed by testicular germ cells. Part 4: intercellular bridges, mitochondria, nuclear envelope, apoptosis, ubiquitination, membrane/voltage-gated channels, methylation/acetylation, and transcription factors. Microsc. Res. Tech. *73*, 364–408. https://doi.org/10.1002/jemt.20785.
9. Kwon, Y.T., and Ciechanover, A. (2017). The Ubiquitin Code in the Ubiquitin-Proteasome System and Autophagy. Trends Biochem. Sci. *42*, 873–886. https://doi.org/10.1016/j.tibs.2017.09.002.
10. Nijman, S.M.B., Luna-Vargas, M.P.A., Velds, A., Brummelkamp, T.R., Dirac, A.M.G., Sixma, T.K., and Bernards, R. (2005). A genomic and functional inventory of deubiquitinating enzymes. Cell *123*, 773–786. https://doi.org/10.1016/j.cell.2005.11.007.
11. Richburg, J.H., Myers, J.L., and Bratton, S.B. (2014). The role of E3 ligases in the ubiquitin-dependent regulation of spermatogenesis. Semin. Cell Dev. Biol. *30*, 27–35. https://doi.org/10.1016/j.semcdb.2014.03.001.
12. Suresh, B., Lee, J., Hong, S.H., Kim, K.S., and Ramakrishna, S. (2015). The role of deubiquitinating enzymes in spermatogenesis. Cell. Mol. Life Sci. *72*, 4711–4720. https://doi.org/10.1007/s00018-015-2030-z.
13. Komander, D., Clague, M.J., and Urbé, S. (2009). Breaking the chains: structure and function of the deubiquitinases. Nat. Rev. Mol. Cell Biol. *10*, 550–563. https://doi.org/10.1038/nrm2731.
14. Cohn, M.A., Kowal, P., Yang, K., Haas, W., Huang, T.T., Gygi, S.P., and D'Andrea, A.D. (2007). A UAF1-containing multisubunit protein complex regulates the Fanconi anemia pathway. Mol. Cell *28*, 786–797. https://doi.org/10.1016/j.molcel.2007.09.031.
15. Williams, S.A., Maecker, H.L., French, D.M., Liu, J., Gregg, A., Silverstein, L.B., Cao, T.C., Carano, R.A.D., and Dixit, V.M. (2011). USP1 deubiquitinates ID proteins to preserve a mesenchymal stem cell program in osteosarcoma. Cell *146*, 918–930. https://doi.org/10.1016/j.cell.2011.07.040.
16. Yu, Z., Song, H., Jia, M., Zhang, J., Wang, W., Li, Q., Zhang, L., and Zhao, W. (2017). USP1-UAF1 deubiquitinase complex stabilizes TBK1 and enhances antiviral responses. J. Exp. Med. *214*, 3553–3563. https://doi.org/10.1084/jem.20170180.
17. Song, H., Zhao, C., Yu, Z., Li, Q., Yan, R., Qin, Y., Jia, M., and Zhao, W. (2020). UAF1 deubiquitinase complexes facilitate NLRP3 inflammasome activation by promoting NLRP3 expression. Nat. Commun. *11*, 6042. https://doi.org/10.1038/s41467-020-19939-8.
18. Cohn, M.A., Kee, Y., Haas, W., Gygi, S.P., and D'Andrea, A.D. (2009). UAF1 is a subunit of multiple deubiquitinating enzyme complexes. J. Biol. Chem. *284*, 5343–5351. https://doi.org/10.1074/jbc.M808430200.
19. Sowa, M.E., Bennett, E.J., Gygi, S.P., and Harper, J.W. (2009). Defining the human deubiquitinating enzyme interaction landscape. Cell *138*, 389–403. https://doi.org/10.1016/j.cell.2009.04.042.
20. Yang, K., Moldovan, G.L., Vinciguerra, P., Murai, J., Takeda, S., and D'Andrea, A.D.

(2011). Regulation of the Fanconi anemia pathway by a SUMO-like delivery network. Genes Dev. *25*, 1847–1858. https://doi.org/10.1101/gad.17020911.

21. Park, E., Kim, J.M., Primack, B., Weinstock, D.M., Moreau, L.A., Parmar, K., and D'Andrea, A.D. (2013). Inactivation of Uaf1 causes defective homologous recombination and early embryonic lethality in mice. Mol. Cell Biol. *33*, 4360–4370. https://doi.org/10.1128/MCB.00870-13.
22. Kim, J.M., Parmar, K., Huang, M., Weinstock, D.M., Ruit, C.A., Kutok, J.L., and D'Andrea, A.D. (2009). Inactivation of murine Usp1 results in genomic instability and a Fanconi anemia phenotype. Dev. Cell *16*, 314–320. https://doi.org/10.1016/j.devcel.2009.01.001.
23. Chen, Y., Zheng, Y., Gao, Y., Lin, Z., Yang, S., Wang, T., Wang, Q., Xie, N., Hua, R., Liu, M., et al. (2018). Single-cell RNA-seq uncovers dynamic processes and critical regulators in mouse spermatogenesis. Cell Res. *28*, 879–896. https://doi.org/10.1038/s41422-018-0074-y.
24. Griswold, M.D. (2016). Spermatogenesis: The Commitment to Meiosis. Physiol. Rev. *96*, 1–17. https://doi.org/10.1152/physrev.00013.2015.
25. Oakberg, E.F. (1956). Duration of spermatogenesis in the mouse and timing of stages of the cycle of the seminiferous epithelium. Am. J. Anat. *99*, 507–516. https://doi.org/10.1002/aja.1000990307.
26. Oakberg, E.F. (1956). A description of spermiogenesis in the mouse and its use in analysis of the cycle of the seminiferous epithelium and germ cell renewal. Am. J. Anat. *99*, 391–413. https://doi.org/10.1002/aja.1000990303.
27. Meistrich, M.L., and Hess, R.A. (2013). Assessment of spermatogenesis through staging of seminiferous tubules. Methods Mol. Biol. *927*, 299–307. https://doi.org/10.1007/978-1-62703-038-0_27.
28. Nakata, H., Wakayama, T., Takai, Y., and Iseki, S. (2015). Quantitative analysis of the cellular composition in seminiferous tubules in normal and genetically modified infertile mice. J. Histochem. Cytochem. *63*, 99–113. https://doi.org/10.1369/0022155414562045.
29. Lin, Z., Hsu, P.J., Xing, X., Fang, J., Lu, Z., Zou, Q., Zhang, K.J., Zhang, X., Zhou, Y., Zhang, T., et al. (2017). Mettl3-/Mettl14-mediated mRNA N(6)-methyladenosine modulates murine spermatogenesis. Cell Res. *27*, 1216–1230. https://doi.org/10.1038/cr.2017.117.
30. Garcia-Santisteban, I., Zorroza, K., and Rodriguez, J.A. (2012). Two nuclear localization signals in USP1 mediate nuclear import of the USP1/UAF1 complex. PLoS One *7*, e38570. https://doi.org/10.1371/journal.pone.0038570.
31. Bose, R., Manku, G., Culty, M., and Wing, S.S. (2014). Ubiquitin-proteasome system in spermatogenesis. Adv. Exp. Med. Biol. *759*, 181–213. https://doi.org/10.1007/978-1-4939-0817-2_9.
32. Xiong, Y., Yu, C., and Zhang, Q. (2022). Ubiquitin-Proteasome System-Regulated Protein Degradation in Spermatogenesis. Cells *11*. https://doi.org/10.3390/cells11061058.
33. Villamil, M.A., Liang, Q., and Zhuang, Z. (2013). The WD40-repeat protein-containing deubiquitinase complex: catalysis, regulation, and potential for therapeutic intervention. Cell Biochem. Biophys. *67*, 111–126. https://doi.org/10.1007/s12013-013-9637-1.
34. Nijman, S.M.B., Huang, T.T., Dirac, A.M.G., Brummelkamp, T.R., Kerkhoven, R.M., D'Andrea, A.D., and Bernards, R. (2005). The deubiquitinating enzyme USP1 regulates the Fanconi anemia pathway. Mol. Cell *17*, 331–339. https://doi.org/10.1016/j.molcel.2005.01.008.
35. Sourisseau, T., Helissey, C., Lefebvre, C., Ponsonnailles, F., Malka-Mahieu, H., Olaussen, K.A., André, F., Vagner, S., and Soria, J.C. (2016). Translational regulation of the mRNA encoding the ubiquitin peptidase USP1 involved in the DNA damage response as a determinant of Cisplatin resistance. Cell Cycle *15*, 295–302. https://doi.org/10.1080/15384101.2015.1120918.
36. García-Santisteban, I., Peters, G.J., Giovannetti, E., and Rodríguez, J.A. (2013). USP1 deubiquitinase: cellular functions, regulatory mechanisms and emerging potential as target in cancer therapy. Mol. Cancer *12*, 91. https://doi.org/10.1186/1476-4598-12-91.
37. Gagnon, D., Lehoux, M., and Archambault, J. (2015). Artificial Recruitment of UAF1-USP Complexes by a PHLPP1-E1 Chimeric Helicase Enhances Human Papillomavirus DNA Replication. J. Virol. *89*, 6227–6239. https://doi.org/10.1128/JVI.00560-15.
38. Gangula, N.R., and Maddika, S. (2013). WD repeat protein WDR48 in complex with deubiquitinase USP12 suppresses Akt-dependent cell survival signaling by stabilizing PH domain leucine-rich repeat protein phosphatase 1 (PHLPP1). J. Biol. Chem. *288*, 34545–34554. https://doi.org/10.1074/jbc.M113.503383.
39. Li, H., Lim, K.S., Kim, H., Hinds, T.R., Jo, U., Mao, H., Weller, C.E., Sun, J., Chatterjee, C., D'Andrea, A.D., and Zheng, N. (2016). Allosteric Activation of Ubiquitin-Specific Proteases by beta-Propeller Proteins UAF1 and WDR20. Mol. Cell *63*, 249–260. https://doi.org/10.1016/j.molcel.2016.05.031.
40. Kee, Y., Yang, K., Cohn, M.A., Haas, W., Gygi, S.P., and D'Andrea, A.D. (2010). WDR20 regulates activity of the USP12 x UAF1 deubiquitinating enzyme complex. J. Biol. Chem. *285*, 11252–11257. https://doi.org/10.1074/jbc.M109.095141.
41. Dahlberg, C.L., and Juo, P. (2014). The WD40-repeat proteins WDR-20 and WDR-48 bind and activate the deubiquitinating enzyme USP-46 to promote the abundance of the glutamate receptor GLR-1 in the ventral nerve cord of Caenorhabditis elegans. J. Biol. Chem. *289*, 3444–3456. https://doi.org/10.1074/jbc.M113.507541.
42. Liang, Q., Dexheimer, T.S., Zhang, P., Rosenthal, A.S., Villamil, M.A., You, C., Zhang, Q., Chen, J., Ott, C.A., Sun, H., et al. (2014). A selective USP1-UAF1 inhibitor links deubiquitination to DNA damage responses. Nat. Chem. Biol. *10*, 298–304. https://doi.org/10.1038/nchembio.1455.
43. Houghtaling, S., Timmers, C., Noll, M., Finegold, M.J., Jones, S.N., Meyn, M.S., and Grompe, M. (2003). Epithelial cancer in Fanconi anemia complementation group D2 (Fancd2) knockout mice. Genes Dev. *17*, 2021–2035. https://doi.org/10.1101/gad.1103403.
44. Roa, S., Avdievich, E., Peled, J.U., Maccarthy, T., Werling, U., Kuang, F.L., Kan, R., Zhao, C., Bergman, A., Cohen, P.E., et al. (2008). Ubiquitylated PCNA plays a role in somatic hypermutation and class-switch recombination and is required for meiotic progression. Proc. Natl. Acad. Sci. USA *105*, 16248–16253. https://doi.org/10.1073/pnas.0808182105.
45. Abe, H., Alavattam, K.G., Hu, Y.C., Pang, Q., Andreassen, P.R., Hegde, R.S., and Namekawa, S.H. (2020). The Initiation of Meiotic Sex Chromosome Inactivation Sequesters DNA Damage Signaling from Autosomes in Mouse Spermatogenesis. Curr. Biol. *30*, 408–420.e5. https://doi.org/10.1016/j.cub.2019.11.064.
46. Menon, D.U., Kirsanov, O., Geyer, C.B., and Magnuson, T. (2021). Mammalian SWI/SNF chromatin remodeler is essential for reductional meiosis in males. Nat. Commun. *12*, 6581. https://doi.org/10.1038/s41467-021-26828-1.
47. Wang, H., Zhao, R., Guo, C., Jiang, S., Yang, J., Xu, Y., Liu, Y., Fan, L., Xiong, W., Ma, J., et al. (2016). Knockout of BRD7 results in impaired spermatogenesis and male infertility. Sci. Rep. *6*, 21776. https://doi.org/10.1038/srep21776.
48. Obholz, K.L., Akopyan, A., Waymire, K.G., and MacGregor, G.R. (2006). FNDC3A is required for adhesion between spermatids and Sertoli cells. Dev. Biol. *298*, 498–513. https://doi.org/10.1016/j.ydbio.2006.06.054.
49. Liu, C., Song, Z., Wang, L., Yu, H., Liu, W., Shang, Y., Xu, Z., Zhao, H., Gao, F., Wen, J., et al. (2017). Sirt1 regulates acrosome biogenesis by modulating autophagic flux during spermiogenesis in mice. Development *144*, 441–451. https://doi.org/10.1242/dev.147074.
50. Guidi, L.G., Holloway, Z.G., Arnoult, C., Ray, P.F., Monaco, A.P., Molnár, Z., and Velayos-Baeza, A. (2018). AU040320 deficiency leads to disruption of acrosome biogenesis and infertility in homozygous mutant mice. Sci. Rep. *8*, 10379. https://doi.org/10.1038/s41598-018-28666-6.
51. Bastos, H., Lassalle, B., Chicheportiche, A., Riou, L., Testart, J., Allemand, I., and Fouchet, P. (2005). Flow cytometric characterization of viable meiotic and postmeiotic cells by Hoechst 33342 in mouse spermatogenesis. Cytometry A. *65*, 40–49. https://doi.org/10.1002/cyto.a.20129.
52. Struijk, R.B., De Winter-Korver, C.M., van Daalen, S.K.M., Hooibrink, B., Repping, S., and van Pelt, A.M.M. (2019). Simultaneous Purification of Round and Elongated Spermatids from Testis Tissue Using a FACS-Based DNA Ploidy Assay. Cytometry A. *95*, 309–313. https://doi.org/10.1002/cyto.a.23698.

STAR★METHODS

KEY RESOURCES TABLE

REAGENT or RESOURCE	SOURCE	IDENTIFIER
Antibodies		
WDR48 Polyclonal antibody	Proteintech	Cat# 16503-1-AP; RRID: AB_2878266
Anti-WDR48 antibody produced in rabbit	Sigma-Aldrich	Cat# HPA058015; RRID: AB_2683580
WDR48 (E-4): sc-514473	Santa Cruz	Cat# sc-514473;
USP1 Polyclonal antibody	Proteintech	Cat# 14346-1-AP; RRID: AB_2214314
KDM3A,JMJD1A Polyclonal antibody	Proteintech	Cat# 12835-1-AP; RRID: AB_1072935
BRDT antibody [C3], C-term	GeneTex	Cat# GTX100201; RRID: AB_1240521
MORC3 Polyclonal antibody	Proteintech	Cat# 24994-1-AP; RRID: AB_2879836
Anti-FANCD2 antibody [EPR2302]	Abcam	Cat# ab108928; RRID: AB_10862535
PCNA Antibody (PC10)	Santa Cruz	Cat# sc-56; RRID: AB_628110
HA-Tag (C29F4) Rabbit mAb	Cell Signaling Technology	Cat# 3724; RRID: AB_1549585
Rabbit Anti-DDX4/VASA	Abcam	Cat# ab13840; RRID:AB_443012
Beta Actin Monoclonal antibody	Proteintech	Cat# 66009-1-Ig; RRID: AB_2687938
Lamin B1 Polyclonal antibody	Proteintech	Cat# 12987-1-AP; RRID: AB_2136290
Goat Anti-Rabbit IgG H&L (Alexa Fluor 488)	Abcam	Cat# ab150077; RRID: AB_2630356
Goat Anti-Rabbit IgG H&L (Alexa Fluor 594)	Abcam	Cat# ab150084; RRID: AB_2734147
Goat Anti-Mouse IgG H&L (Alexa Fluor 488)	Abcam	Cat# ab150113; RRID: AB_2576208
Goat Anti-Mouse IgG H&L (Alexa Fluor 594)	Abcam	Cat# ab150120; RRID: AB_2631447
Chemicals, peptides, and recombinant proteins		
Bouin's solution	Sigma	Cat# HT10132
Paraformaldehyde,4%	Solarbio	Cat# P1110
Glutaraldehyde	Aladdin	Cat# G105907
Triton X-100	Sigma	Cat# T9284
Lectin PNA, Alexa Fluor 594 Conjugate	Thermo Fisher Scientific	Cat# L32459
Rabbit IgG	Abmart	Cat# B30011S
DAPI	Vector Laboratories	Cat# H-1200
Hoechst 33342	Thermo Fisher Scientific	Cat# H1399
cOmplete Protease Inhibitor	Roche	Cat# 04693116001
Protein A agarose	Roche	Cat# 11719408001
Protein G agarose	Roche	Cat# 11719416001
Critical commercial assays		
TUNEL KIT	keyGEN BioTECH	Cat# KGA7072
Double-Fluorescence immunohistochemical mouse/rabbit kit	Immunoway	Cat# RS0036
Periodic Acid Schiff (PAS) Stain Kit (Mucin Stain)	Abcam	Cat# ab150680
Deposited data		
Proteomic data of round spermatids from WT and *Uaf1* sKO mice	ProteomeXchange	PXD046120
Experimental models: Organisms/strains		
Mouse: C57BL/6J	Beijing Vital River Laboratory Animal Technology Co.	Strain Code: 219

(*Continued on next page*)

Continued

REAGENT or RESOURCE	SOURCE	IDENTIFIER
Mouse: *Uaf1*$^{flox/flox}$	This paper	N/A
Mouse: *Stra8-Cre*	Lin et al.[29]	N/A
Mouse: UAF1-C-HA	This paper	N/A
Oligonucleotides		
primers used in this study are listed in Table S1	This study	N/A
Software and algorithms		
GraphPad Prism	GraphPad	RRID: SCR_002798
CellSens	Olympus	RRID: SCR_014551

RESOURCE AVAILABILITY

Lead contact

Further information and requests for resources should be directed to and will be fulfilled by the lead contact, Hongbin Liu (hongbin_sduivf@aliyun.com).

Materials availability

Mouse lines generated in this study are available from the lead contact upon request with a completed Materials Transfer Agreement.

Data and code availability

- Proteomic data have been deposited at ProteomeXchange and are publicly available as of the date of publication.
- The accession number for the raw and processed data files is PXD046120.
- Any additional information required to reanalyze the data reported in this paper is available from the lead contact upon request.

EXPERIMENTAL MODEL AND STUDY PARTICIPANT DETAILS

Uaf1$^{flox/flox}$ mice in a C57BL/6J background were generated by Cyagen Biosciences Inc. (Guangzhou, China) using CRISPR-Pro technology. The *Stra8-GFPCre* lines were generated by Shanghai Biomodel Organism Co., Ltd. All mice described above were maintained in the C57BL/6J (B6) background. *Uaf1*$^{flox/flox}$ mice were crossed with Stra8-GFPCre knockin mice to obtain *Uaf1*$^{fl/-}$*; Stra8-Cre* mice with *Uaf1* deficiency in germ cells, resulting in *Uaf1*-deficient mice (*Uaf1* sKO mice) with 984 missing base pairs (6350–7334, containing the third exon of the *Uaf1* gene NM_026236.3), which caused a frameshift mutation. For animal experiments with *Uaf1* sKO mice, littermate controls with normal *Uaf1* expression (*Uaf1*$^{fl/fl}$) were used. All animal experiments were performed in accordance with the National Institute of Health Guide for the Care and Use of Laboratory Animals, and approval was obtained from the Scientific Investigation Board of the Medical School of Shandong University (Jinan, Shandong Province, China). UAF1-C-HA mice were supplied by the Genome Tagging Project (GTP) Center, CEMCS, CAS, which was supported by the Shanghai Municipal Commission for Science and Technology Grants (19411951800). The HA protein was added to the C-terminal of the UAF1 protein using CRISPR/Cas9 technology without affecting the expression of UAF1 protein. Male mice were used for immunoprecipitation of testis extracts, histological analysis of testes, immunostaining of testes, transmission electron microscopy, and proteomic experiments (age: 24–45 days old, 8-week-old and 12-week-old mice). Female mice were used for immunoprecipitation of ovary extracts, histological analysis of the ovaries, and immunostaining experiments (age: 3-month-old, 6-month-old). All the animals were housed in a specific pathogen-free facility with 40–70% humidity and daily cycles of 12 h of light at 23°C and 12 h of dark at 21°C.

METHOD DETAILS

Histology, immunostaining, TEM, TUNEL assay

For histology, 5 μm paraffin-embedded sections of testes and epididymides were prepared and then stained with periodic acid-shiff (PAS) and/or hematoxylin. Stages of seminiferous epithelium cycle and steps of spermatid development were based on the morphology of the acrosome and the nucleus of germ cells.[1]

For TEM, testes sections were fixed with 2.5% phosphate buffered glutaraldehyde. The testes samples were then dehydrated with an ethanol gradient (50%, 70%, 90% and 100%) and subsequently infiltrated with 100% acetone. After embedding in Epon 812, the testes samples were sliced by an ultramicrotome and stained with uranyl acetate and lead citrate. The testes samples were then observed and photographed on a transmission electron microscope (TECNAI-10, Philips) with an accelerating voltage of 80 kV.

For immunostaining, testicular sections were fixed with 4% paraformaldehyde, permeabilized with 0.2% Triton X-100 in PBS, and incubated with primary antibodies. Primary antibodies used for immunofluorescence were as follows: rabbit anti-UAF1 (1:200 dilution; Millipore #

HPA058015), rabbit anti-UAF1 (1:200 dilution; PTG # 16503-1-AP), rabbit anti-USP1 (1:200 dilution; PTG # 14346-1-AP). Primary antibodies were detected with Alexa Fluor 488- or 594-conjugated secondary antibodies (1:500 dilution; Abcam #ab150084, #ab150077, #ab150113, and #ab150120) for 1 h at room temperature. The slides were washed several times with PBS and mounted using Vectashield antifade mounting medium with DAPI (Vector Laboratories, #H-1200). The immunofluorescence images were taken immediately using a 780/710 laser scanning microscope (Zeiss) or SP8 microscope (Leica).

For TUNEL staining, we followed the manufacturer's instructions (keyGEN BioTECH, #KGA7072).

CASA

The sperm samples from at least three WT and *Uaf1* sKO for each genotype were used for sperm motility assessment analysis using an Olympus B×51 microscope (Olympus, Tokyo, Japan) through a 20× phase objective. A 10 μL sperm sample was taken and placed into 80 mm deep glass cell chambers (Hamilton Thorne, 80 mm 2X-CEI), and images were obtained with a CCD camera. CASA was performed on more than 200 spermatozoa using the Animal Motility System (Hamilton Thorne, Beverly, MA, USA). The semen analysis was replicated at least five times.

Western blotting

To prepare extracts, tissues were collected from male C57BL/6 mice and suspended in lysis buffer [50 mM HEPES-KOH (pH 7.5), 100 mM KCl, 2 mM EDTA, 10% glycerol, 0.1% NP-40, 10 mM NaF, 0.25 mM Na3VO4, and 50 mM β-glycerolphosphate] supplemented with cOmplete Protease Inhibitor (Roche #04693116001). After homogenization, the cell extracts were centrifuged at 13,000× *g* for 20 min at 4°C. The supernatant extracts were used for immunoprecipitation and Western blots. Equal amounts of protein were electrophoresed on 10% SDS–polyacrylamide gels, and the bands were transferred to polyvinylidene fluoride membranes (Millipore, USA). Immunoreactive bands were detected and analyzed with a Bio-Rad ChemiDoc MP imaging System and Image Lab Software (Bio-Rad, USA). Relative protein levels in each sample were normalized to β-Actin to standardize the loading variations. The primary antibodies for immunoblotting included anti-β-Actin (1:10,000 dilution; PTG, # 66009-1-Ig), anti-Lamin-B1 (1:3000 dilution; PTG # 12987-1-AP), anti-UAF1 (1:1000 dilution; PTG # 16503-1-AP), anti-USP1 (1:1000 dilution; PTG # 14346-1-AP), anti-KDM3A (1:1000, PTG # 12835-1-AP), anti-BRDT (1:1000, GeneTex # GTX100201), anti-MORC3 (1:1000 dilution; PTG #24994-1-AP), anti-FANCD2 (1:1000 dilution; Abcam # ab108928), and anti-PCNA (1:1000 dilution; Santa Cruz # SC56).

Immunoprecipitation

Immunoprecipitation was performed with 8-week-old testes protein extracts using anti-UAF1 (1:100 dilution), anti-USP1 (1:100 dilution), anti-HA (1:100 dilution) antibodies. Antibodies and WT and *Uaf1* sKO testes extracts were incubated overnight at 4°C, followed by incubation with protein A agarose (Roche, #11719408001) and protein G agarose (Roche, #11719416001) for 1 hour at 4°C. After washing, the beads were loaded onto 4–20% Tris-Glycine Mini Gels (Invitrogen) and separated proteins were detected by western blotting with the indicated antibodies. Immunoprecipitations were performed using rabbit anti- HA antibody (Cell Signaling Technology # 3724) and rabbit anti-IgG antibody (Abmart # B30011S). The Western blots were repeated at least three times.

Fluorescence-activated cell sorting of round spermatids

Fluorescence-activated cell sorting (FACS) purification was conducted to collect round spermatids from 8-week-old WT and *Uaf1* sKO mice for proteomics.[51,52] After removing the tunica albuginea, the testes were placed in 5 ml PBS containing collagenase type I (120 U/ml) and mixed for 10 min at 35°C. The testes were digested in 5 ml of 0.25% trypsin plus 0.1 ml of deoxyribonuclease I (5 mg/ml) at 35°C for 8 min, and the reaction was terminated by the addition of 0.5 ml fetal bovine serum. The suspension was passed through a 70 μm honeycomb filter, and the cell suspension was centrifuged the cell suspension at 4°C at 500× *g* for 5 min. The supernatant was removed and the cell pellet was resuspended in 1 ml DMEM with 40 μg Hoechst 33342, 2 μl Zombie NIR™ dye, and 5 μl DNase I. The cell suspension was stirred at 34°C for 20 min, then centrifuged at 500× *g* for 5 min at 4°C and resuspended in PBS at a concentration of 10^5 ml for sorting. Populations of fluorescently labelled cells were collected according to the sorting channel into 1.5-ml LoBind microcentrifuge tubes (Eppendorf, 022431021) containing 0.5 mL PBS. The cell suspension was centrifuged and some of the supernatant was removed leaving about 10μl PBS.

Proteomic analysis

Round spermatids for proteomic analysis were obtained from 8-week-old C57BL/6 male mice and subjected to LC-MS/MS analysis following a standard protocol. In brief: (1) FACS purification was conducted to collect round spermatids from 8-week-old WT and *Uaf1* sKO mice. Round spermatids were transferred to tubes containing lysis buffer (1% Protease Inhibitor Cocktail) on ice. After homogenization, the cell extracts were centrifuged at 13,000× *g* for 20 min at 4°C. The supernatant was collected after centrifugation, and the protein concentration was determined. After trypsin digestion and purification, peptides were reconstituted in 0.5 M TEAB and processed according to the manufacturer's protocol using the TMT kit. Released peptides were subjected to LCMS/MS identification and quantification on a Thermo Scientific LTQ Orbitrap XL mass spectrometer (Thermo Fisher Scientific) with a Finnigan Nanospray II electrospray ionization source. The raw data were processed using Domain Annotation (InterProScan), GO Annotation (http://www.ebi.ac.uk/GOA/), and KEGG Pathway Annotation (KEGG online service tools KAAS mapper).

QUANTIFICATION AND STATISTICAL ANALYSIS

Bioinformatics analysis

Differentially abundant proteins were identified using 1.3-fold change and a threshold of $p < 0.05$ for the Wilcoxon test. Subsequently, multiple bioinformatics tools were performed to analyze these proteins. The Kyoto Encyclopedia of Genes and Genomes (KEGG) database was used to analyze enriched pathways. The R package clusterProfiler and Metascape (http://metascape.org) were used for Gene Ontology (GO) and KEGG pathways enrichment analyses. For GO and KEGG enrichment analyses, two-tailed Fisher's exact test was applied to assess differentially abundant proteins against all identified proteins. Results with a corrected $p < 0.05$ were considered significant.

We also used the Power Law Global Error Model (PLGEM) to analyze proteomics data. First, we calculated the signal-to-noise ratio (STN), because it explicitly takes into account unequal variances and penalizes proteins that have higher variance in each class more than those proteins that have a high variance in one class and a low variance in another. PLGEM can only be fitted on a set of replicates of the same experimental condition, so we needed to select the condition for the fitting step. In our dataset, there are two conditions: "WT" and "sKO"; we chose "sKO" (i.e., fitCondition = "sKO"). We then proceeded with the resampled STNs and calculated differences with corresponding p values between the two conditions. We used ggplot2 to create an expression volcano plot to visualize the results obtained from PLGEM.

Statistical analyses

Statistical data are presented as the mean $\pm$ standard error of the mean. Most experiments included at least three independent samples and were repeated at least three times. A two-tailed unpaired Student's *t* test was used to compare the results of the two experimental groups. Using the two-tailed Student's *t* test, $p < 0.05$, $p < 0.01$, and $p < 0.001$ were considered statistically significant and are represented by asterisks (*), (**), and (***), respectively. "n.s." indicates non-significant.